

Predictive value of [^{18}F]-fluoride PET for monitoring bone remodeling in patients with orthopedic conditions treated with a Taylor spatial frame

Alejandro Sanchez-Crespo^{1,2} · Frederik Christiansson³ · Charlotte Karlsson Thur⁴ · Henrik Lundblad⁴ · Anders Sundin⁵

Received: 28 December 2015 / Accepted: 5 July 2016 / Published online: 23 July 2016
© Springer-Verlag Berlin Heidelberg 2016

Abstract

Purpose The Taylor Spatial Frame (TSF) is used to correct orthopedic conditions such as correction osteotomies in delayed fracture healing and pseudarthrosis. Long-term TSF-treatments are common and may lead to complications. Current conventional radiological methods are often unsatisfactory for therapy monitoring. Hence, an imaging technique capable of quantifying bone healing progression would be advantageous.

Methods A cohort of 24 patients with different orthopedic conditions, pseudarthrosis ($n = 10$), deformities subjected to correction osteotomy ($n = 9$), and fracture ($n = 5$) underwent dynamic [^{18}F]-fluoride (Na^{18}F) PET/CT at 8 weeks and 4 months, respectively, after application of a TSF. Parametric images, corresponding to the net transport rate of [^{18}F]-fluoride from plasma to bone, K_i were calculated. The ratio of the maximum K_i at PET scan 2 and 1 ($\overline{K}_{i,\max}$) as well as the ratio of the maximum Standard Uptake Value at PET scan 2 and 1 (\overline{SUV}_{\max}) were calculated for each individual. Different treatment end-points were scored, and the overall

treatment outcome score was compared with the osteoblastic activity progression as scored with $\overline{K}_{i,\max}$ or \overline{SUV}_{\max} .

Results $\overline{K}_{i,\max}$ and \overline{SUV}_{\max} were not correlated within each orthopedic group ($p > 0.1$ for all groups), nor for the pooled population ($p = 0.12$). The distribution of $\overline{K}_{i,\max}$ was found significantly different among the different orthopedic groups ($p = 0.0046$) -also for \overline{SUV}_{\max} ($p = 0.022$). The positive and negative treatment predictive values for $\overline{K}_{i,\max}$ were 66.7 % and 77.8 %, respectively. Corresponding values for \overline{SUV}_{\max} were 25 % and 33.3 %

Conclusions The $\overline{K}_{i,\max}$ obtained from dynamic [^{18}F]-fluoride-PET imaging is a promising predictive factor to evaluate changes in bone healing in response to TSF treatment.

Keywords PET/CT · Parametric PET imaging · TSF · Fluoride · Influx rate · SUV

Introduction

The circular external fixator with adjustable struts, the Taylor Spatial Frame (TSF) [1–3], is generally used to correct and treat different orthopedic conditions such as bone deformities, fractures or unhealed pseudarthrosis. However, long-term treatment with TSF may be subject to complications. Conventional radiological methods are not infrequently unsatisfactory for therapy monitoring and early identification of treatment failure.

Currently, a serial planar X-ray is routinely used for follow-up of bone healing to monitor formation of callus. However, detection of callus formation on X-ray can be difficult and is subject to the observer's experience. Computed tomography (CT) has, therefore, been suggested to replace conventional radiography to evaluate bone healing, because it offers better

✉ Alejandro Sanchez-Crespo
alejandro.sanchez-crespo@karolinska.se

¹ Department of Hospital Physics, Nuclear medicine, Karolinska University Hospital, Stockholm, Sweden

² Karolinska University Hospital, Nuklearmedicin A3:01, S-171 76 Stockholm, Sweden

³ Department of Radiology, Nyköping Hospital, Nyköping, Sweden

⁴ Department of Molecular Medicine and Surgery, Karolinska Institutet, Stockholm, Sweden

⁵ Department of Radiology and Molecular Imaging, Uppsala University Hospital, Uppsala, Sweden

visualization [4], although metal artifacts from the TSF may sometimes hamper the evaluation [5, 6]. Other morphological imaging modalities like magnetic resonance imaging (MRI) and ultrasound have not been found to facilitate the early prediction of delayed healing in long bone fracture non-unions [7]. Hence, there is a need for a better diagnostic tool that can offer an objective measure of the bone healing process in order to detect delayed or arrested bone healing at an early stage. This would change the patient management as well as the outcome of the treatment, by, for example, avoiding prolonged fixation or even further surgery.

The use of PET as a diagnostic tool for bone healing in patients with a TSF is attractive because it can provide a direct quantitative assessment of metabolic progression of the orthopedic condition. In this respect, [^{18}F]-fluoride (Na^{18}F) PET has previously been used to study bone metabolism in different metabolic bone disorders [8] and to monitor therapeutic response [9]. As osteoblasts and osteoclasts are activated at the site of bone formation, fluoride ions are incorporated into the bone by exchange with the hydroxyl ions in bone crystals. Bone metabolic activity measured with [^{18}F]-fluoride PET has previously been reported to correlate well with bone histomorphometry [10, 11]. However, the well-known PET quantifier, standardized uptake value (SUV), suitable for inter-patient and inter-study comparison in PET studies of tumor glucose metabolism using [^{18}F]-fluoro-deoxy-glucose, has not yet been recognized as a validated tool for [^{18}F]-fluoride quantification in clinical studies [12–14]. A more interesting approach for [^{18}F]-fluoride quantification is instead the use of dynamic PET image analysis and tracer compartment modeling [12–16]. Hawkins et al. 1992 were the first to introduce a three-compartment model to derive the [^{18}F]-fluoride kinetics in dynamic PET image analysis. From this analysis, the net plasma clearance of tracer to bone mineral influx rate (K_i), is generally used to quantify active bone formation. Tracer kinetic parameters can be derived from non-linear fitting of the time activity curves (TAC) obtained at a global level, from analysis of volumes of interest (VOI) or locally, for every image voxel (PET parametric imaging).

The aim of this work was to investigate the predictive value of dynamic [^{18}F]-fluoride-PET parametric imaging in the follow-up and treatment outcome of bone remodeling in adults with three different orthopedic conditions treated with TSF.

Materials and methods

Patients

Twenty-four consecutive patients treated with TSF in the tibia were included in this study. The patients' age ranged from 19–79 (mean 45.2 ± 17.0) years and their weights were 52–130

(mean 79.4 ± 18.2) kg. The patients were divided into three clinical groups, according to their initial orthopedic condition indicating TSF treatment. The three orthopedic conditions included in this study were osteotomy because of deformity ($n = 9$), pseudarthrosis ($n = 1,0$) and fracture ($n = 5$). All patients had normal renal function at the time of the study. The patients did not receive any drugs affecting the whole bone turnover, which could hamper PET image quantification. The TSF was removed from all patients at the time of completing this study. The study was approved by the local ethics and radiation protection committees of the Karolinska University Hospital, Stockholm, Sweden. All patients gave informed consent. Three patients were excluded from the study because they could not complete the study protocol.

[^{18}F]-Fluoride PET/CT study protocol

The patients were examined with [^{18}F]-fluoride PET/CT at two different occasions approximately at 6 to 8 weeks and at 4 months post TSF surgical installation, respectively. All patients were examined on a clinical PET/CT scanner (Biograph 64 TruePoint True V, Siemens Medical Solutions, Erlangen, Germany) according to the same clinical protocol [17]. Each patient underwent a low dose CT (120/140 kVp, 50/60 mAs, 0.5/1.0 s per revolution, pitch 1.0) for PET image attenuation correction and anatomical localization. This was followed by a 45 min single-bed position dynamic PET acquisition in list-mode at the site of the correction for osteotomy, fracture or pseudarthrosis and including the Taylor spatial frame. The PET list-mode acquisition started at the time of the intravenous single bolus administration of 2 MBq of [^{18}F]-fluoride per kilogram of body weight.

Prior to reconstruction, the PET list mode data was separated in 26 consecutive time sinogram-datasets, from injection time, according to; 6×10 , 4×30 , 7×60 , 5×180 and 4×300 (number of frames \times seconds per frame). Sinogram reconstruction was performed using a 2D-OSEM algorithm with four iterations, eight subsets (168×168 matrix), and a 5 mm Gaussian filter with photon scatter and attenuation correction, activity decay, and random coincidence correction.

Reconstruction of the PET parametric images

In this study, a three-compartment model consisting of a vascular compartment (C_{plasma}), an extracellular compartment (C_{extra}), and a compartment of bound fluoride to bone mineral (C_{bound}) was used for the kinetic analysis of [^{18}F]-fluoride bone metabolism [12]. The rate constants describing the transport of [^{18}F]-fluoride between the compartments are K_1 (ml/min/ml) and k_2 (min^{-1}) for forward and reverse transport from C_{plasma} and C_{extra} , respectively, and k_3 (min^{-1}) for the incorporation of [^{18}F]-fluoride to bone C_{bound} . Release of [^{18}F]-fluoride from bone (k_4) is very small compared to the other

rates, and; hence, [¹⁸F]-fluoride transport to bone can be considered an irreversible process without loss of generality [18]. The net transport rate of [¹⁸F]-fluoride from plasma to bone K_i , representing bone osteoblastic activity, can then accurately and independently be estimated [15] according to;

$$K_i = \frac{K_1 k_3}{k_2 + k_3} \text{ (ml/min/ml)} \tag{1}$$

$$\int_0^T PET(x, y, z, t) dt = \frac{K_1 k_3}{k_2 + k_3} \int_0^T \left[\int_0^T C_{Plasma}(t) du \right] dt - \frac{1}{k_2 + k_3} PET(x, y, z, t) + \frac{K_1}{k_2 + k_3} \int_0^T C_{Plasma}(t) dt, \tag{2}$$

where $PET(x,y,z,t)$ is the [¹⁸F]-fluoride activity concentration (Bq/ml) in the PET image at voxel position (x,y,z) and time (t) post administration and $C_{plasma}(t)$ is the partial volume effect (PVE) corrected [¹⁸F]-fluoride TAC in plasma obtained from a VOI in the ipsilateral popliteal artery as the input function. The parameters $\frac{K_1 k_3}{k_2 + k_3}$, $\frac{1}{k_2 + k_3}$ and $\frac{K_1}{k_2 + k_3}$ can then be obtained as the solution of a multilinear least-squared regression ($y = \alpha_1 X_1 + \alpha_2 X_2 + \dots$) at each voxel location. PVE correction of the input function, $C_{plasma}(t)$, was performed by using activity recovery coefficients specifically measured from phantom experiments with the NEMA IEC body phantom as described in [20].

PET images analysis

The maximum value of the net transport rate of [¹⁸F]-fluoride in bone ($K_{i \max}$) in both the ipsilateral (within the tibial osteotomy) and in the contralateral tibia (at the same height as the ipsilateral) were computed from the calculated parametric PET images, $K_{i \max}^{ipsi}$ and $K_{i \max}^{contra}$, respectively. For comparison, the ipsilateral and contralateral maximum standard uptake value, SUV_{\max}^{ipsi} and SUV_{\max}^{contra} respectively, were also obtained from a 5 min static (1-bed-position) PET image acquired 45 min after tracer administration.

The progression in osteoblastic activity 4 months after installation of the TSF was quantified by the ratio of $K_{i \max}^{ipsi}$ between PET scans

$$\bar{K}_{i \max} = \frac{K_{i \max}^{ipsi, PET2}}{K_{i \max}^{ipsi, PET1}} \tag{3}$$

and similarly for the SUV_{\max}^{ipsi}

$$\overline{SUV}_{\max} = \frac{SUV_{\max}^{ipsi, PET2}}{SUV_{\max}^{ipsi, PET1}} \tag{4}$$

The unknown compartment rate constants can be solved with iterative non-linear least-squares methods applied to the time activity concentration curves (TAC) obtained for every PET image voxel. In this work a more general approach is followed by calculating an estimate of K_i for every PET image voxel according to the linearized compartment model solution previously proposed [19].

Statistical data analysis

Relationship between $\bar{K}_{i \max}$ and \overline{SUV}_{\max}

The coefficient of determination between $\bar{K}_{i \max}$ and \overline{SUV}_{\max} for each orthopedic group and pooled data were investigated using Pearson’s linear correlation coefficient.

Relation between osteoblastic activity progression and orthopedic condition

The relation between $\bar{K}_{i \max}$ and the three orthopedic groups of patients was investigated. The Kruskal-Wallis statistics was used to test the null hypothesis that $\bar{K}_{i \max}$ was the same across all three orthopedic groups. The same analysis was performed between \overline{SUV}_{\max} and the three orthopedic groups.

Predictive value of [¹⁸F]-fluoride PET imaging in bone remodeling

To study the predicting value of [¹⁸F]-fluoride PET in bone remodeling, four TSF treatment end points (pain, mobility, infection, and total number of days with the TSF treatment) and one mid-treatment point (callus formation at 4 months) were scored for each patient, as described in Table 1. Patients scoring higher than zero all had a positive outcome of the TSF treatment. Patients scoring less or equal to zero suffer from complications and/or unsuccessful TSF treatment. A confusion matrix was then created with this clinical scoring against $\bar{K}_{i \max}$. An increase in osteoblastic activity with time, corresponding to a $\bar{K}_{i \max} > 1$, was considered as indicative of a positive bone remodeling progression and a decline (or unchanged) in osteoblastic activity with time ($\bar{K}_{i \max} \leq 1$) was considered negative or of no progression. A similar confusion matrix was also built for \overline{SUV}_{\max} under the same assumptions.

Table 1 Clinical parameters and scoring system used to grade the course and outcome of the Taylor spatial frame (TSF) treatment. Callus formation was quantified visually from X-ray images by an experienced radiologist blinded with respect to the PET results. Information about each patient's TSF treatment end-points (pain and infection status, extremity mobility, and treatment duration) were obtained retrospectively from the patient's clinical records

Clinical parameter	Scoring
Callus formation 4 months after TSF installation	-1 absence of callus formation 1 progression of callus formation
Pain status after TSF removal	-1 pain level increases / similar 1 absence of pain
Recovery of mobility after TSF removal	-1 mobility reduction 1 total stability / no mobility reduction
Infection status	-1 positive for infection 1 no infection
Total number of days treated with TSF compared to the average of the group	-1 treatment lasted more days than average 1 treatment lasted fewer days than average

Results

PET parametric images of the influx rate versus SUV images in bone remodeling

The [^{18}F]-fluoride distribution in the affected and the contralateral side at different time points post injection (PI) are shown in Fig. 1. At 10 s PI the [^{18}F]-fluoride was basically in plasma, and; hence, only the arteries were visualized. Interestingly, in the majority of the patients, the tracer bolus delivery on the contralateral side was some seconds delayed (Fig. 1).

Images between 20 and 50 s PI basically represented the extracellular compartment. From 50 s PI and on, the tracer uptake was irreversibly fixed in bone tissue according to the rate Ki . These findings support the accuracy of the three compartment model used in this work to obtain the PET parametric images. The resulting parametric PET data displaying Ki and the corresponding static PET images (summed data 43–45 min PI), in which the radioactivity concentration was recalculated as SUV, are illustrated in Fig. 2a and b, respectively. In the Ki parametric image, tracer uptake in the soft tissues was suppressed and enhanced in bone as compared to the presentation in the static SUV images.

Relationship between $\overline{K}_{i,\max}$ and \overline{SUV}_{\max}

There was no inter-group correlation between $\overline{K}_{i,\max}$ and \overline{SUV}_{\max} coefficients of determination 0.059 ($p = 0.49$), 0.187 ($p = 0.15$), and 0.023 ($p = 0.80$) for the pseudarthrosis, correction osteotomy, and fracture groups, respectively. Also, the pooled data for these three orthopedic conditions showed a poor coefficient of determination between $\overline{K}_{i,\max}$ and \overline{SUV}_{\max} , 0.07 ($p = 0.12$).

Relation between osteoblastic activity progression and orthopedic condition

Figures 3 and 4 show box-plots of the distribution of $\overline{K}_{i,\max}$ and \overline{SUV}_{\max} for the three orthopedic groups, respectively. The

Kruskal-Wallis analysis of this data revealed a highly significant different $\overline{K}_{i,\max}$ distribution between the three orthopedic conditions. The null hypothesis was rejected at a 1 % significance level ($p = 0.0046$). The distribution of \overline{SUV}_{\max} among the different orthopedic conditions was also found significantly different but at the 5 % level ($p = 0.022$). Hence, the $\overline{K}_{i,\max}$ was a better discriminator than \overline{SUV}_{\max} to differ the progression in osteoblastic activity between the three orthopedic conditions.

Predictive value of [^{18}F]-fluoride PET imaging in bone remodeling

Tables 2 and 3 show the confusion matrices for $\overline{K}_{i,\max}$ and \overline{SUV}_{\max} , respectively.

$\overline{K}_{i,\max}$ showed a relatively high sensitivity and specificity of 80 % and 63.6 %, respectively. The corresponding values for \overline{SUV}_{\max} were as low as 33.3 % and 25 %, respectively. The positive predictive value (the ability to predict a complication free total recovery) was 66.7 % for $\overline{K}_{i,\max}$ and only 25 % for \overline{SUV}_{\max} . Even more importantly, the negative predictive value (the ability to predict unsuccessful TSF treatment) was as high as 77.8 % for $\overline{K}_{i,\max}$ and merely 33.3 % for \overline{SUV}_{\max} .

Discussion

In this study, we found that parametric Ki images, derived from dynamic [^{18}F]-fluoride-PET acquisitions, were advantageous to predict bone remodeling during TSF treatment of three orthopedic conditions. The technical considerations during the PET-acquisition have previously been described [17]. A potential problem of examining the patient with a TSF attached is the metal artifacts in the CT images from the frame [5, 6]. However, earlier phantom studies on the impact of the TSF in PET image quantification, revealed that the presence

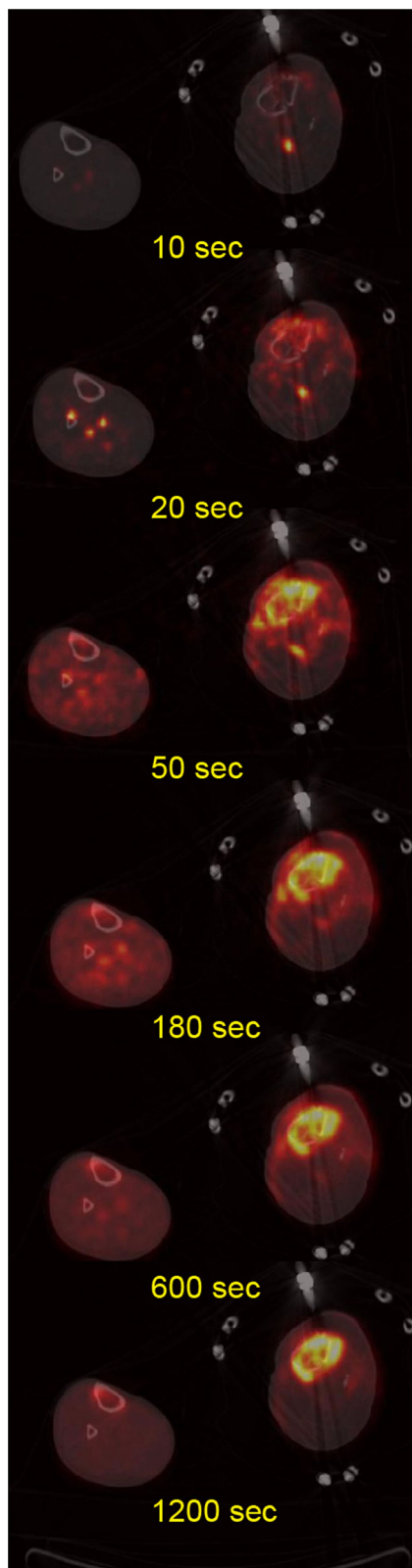


Fig. 1 Transverse PET images from a dynamic acquisition showing the $[^{18}\text{F}]$ -fluoride distribution in a patient with pseudoarthrosis at different time intervals post tracer administration

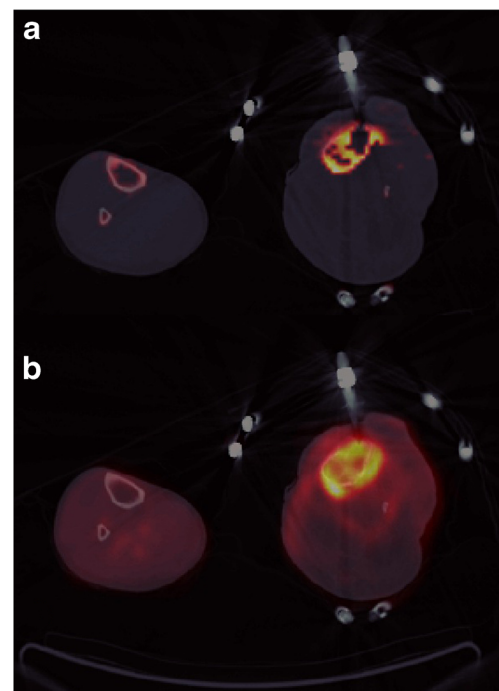
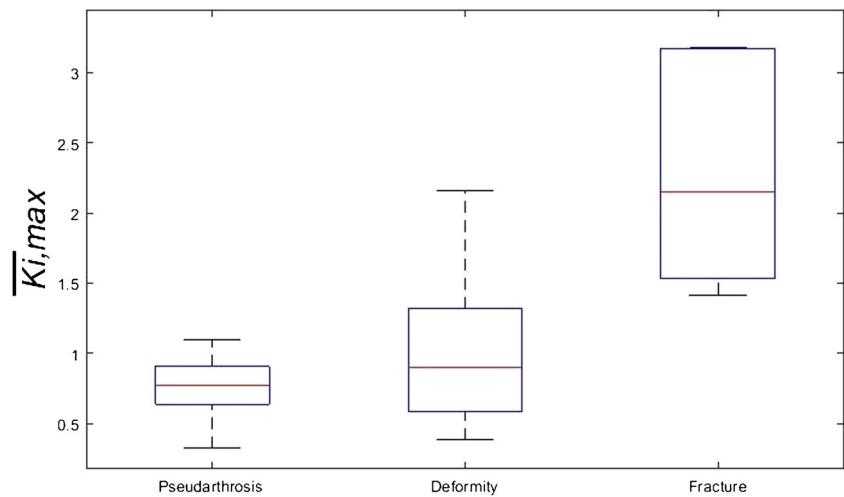


Fig. 2 Transverse PET images of the same patient as in Fig. 1. **a** Parametric image representing the net influx rate constant of $[^{18}\text{F}]$ -fluoride in bone, K_i . **b** Static PET image (data summed 43–45 min post injection) showing radioactivity concentration as SUV

of small metal artifacts from the TSF on the attenuation correction map have a negligible influence on the quantitative properties of the PET images [17].

Another key factor affecting the quality of the calculated parametric K_i -PET images is the definition of the input function. Specifically, in parametric PET imaging, the input function should be taken as close as possible to the tissue region of interest. The reference method is arterial blood sampling from the radial artery, which is invasive and time consuming. Additionally, in the situation in which the distal parts of the patient's legs are examined, the validity of an input function derived from blood collected from the radial artery may be questioned. In this work we, therefore, derived all input functions from the dynamic PET images of the artery closest to the fracture/pseudoarthrosis/correction osteotomy. The fairly large axial field of view of the PET camera used (21 cm) allowed in all patients for including the popliteal artery in the dynamic one-bed-PET examination. The major advantage of this procedure is that the input function will correlate both temporally and spatially with the tracer uptake in the tissue(s) of interest. This is of importance depending on the patient status and the presence of comorbidity in, for example, arteriosclerosis, etc. However, there are major drawbacks when using an image derived input function, the most important being that the activity concentration in plasma and whole blood cannot be separated. This will slightly overestimate the input function used to solve the compartment model. Additionally, the image derived TAC (Bq/ml) obtained from the average activity

Fig. 3 The distribution of the $\overline{K_{i,max}}$ (ratio of the maximum plasma to bone fluoride net influx rate at PET scan 2 and 1), for the three orthopedics groups of patients considered in this work



concentration in the arterial volume of interest (VOI) will be affected by PVE. If not corrected for, PVE reduces the activity concentration in blood and, consequently, it may overestimate the other constant rate factors of the kinetic model.

Generally, there are two main approaches to estimate the net transport rate (K_i) of [^{18}F]-fluoride into bone from dynamic PET data, by non-linear fitting of the TAC of selected VOIs plus an input function or by graphical analysis for irreversible tracers (Patlak plot). The Patlak plot is easily computed, but it requires a linear relation between the variables. It assumes that there is a constant ratio between activity concentration in reversible tissue and plasma. However, this is only achieved after some time post tracer administration. Hence, the precise moment at which steady-state conditions apply is not a priori known, and the reconstruction scheme of the dynamic PET influences the goodness of the Patlak analysis. Further, non-specific binding of the tracer to tissue and plasma proteins affects the Patlak analysis. On the other hand, non-linear fitting of the TAC according to the solution to the

compartment model does not present the same vulnerabilities as the Patlak analysis to the cost of a more computing demanding approach. However, the goodness of the non-linear curve fitting to the TAC depends on the degree of noise in the TAC data.

In this study, the $\overline{K_{i,max}}$ and $\overline{SUV_{max}}$ were not correlated. This is most likely due to bias in the SUV quantification. There are several physical, technical, and biological factors affecting SUV quantification, which are not exclusive for [^{18}F]-fluoride-PET, and that need to be considered, for example, the tracer kinetics and partial volume effects [21]. Further, the SUV metric is basically a measurement of activity concentration in the VOI normalized to administered activity; hence, competitive uptake of the tracer in other compartments of the body may reduce its accuracy. Specifically for [^{18}F]-fluoride as the tracer, the bone SUV quantification in the VOI may vary because of competition for [^{18}F]-fluoride by the kidneys and by the presence of various bone lesions (e.g., osteoarthritis), which may both vary among patients and during the

Fig. 4 The distribution of the $\overline{SUV_{max}}$ (ratio of the maximum Standard Uptake Value at PET scan 2 and 1) for the three orthopedic groups of patients considered in this work

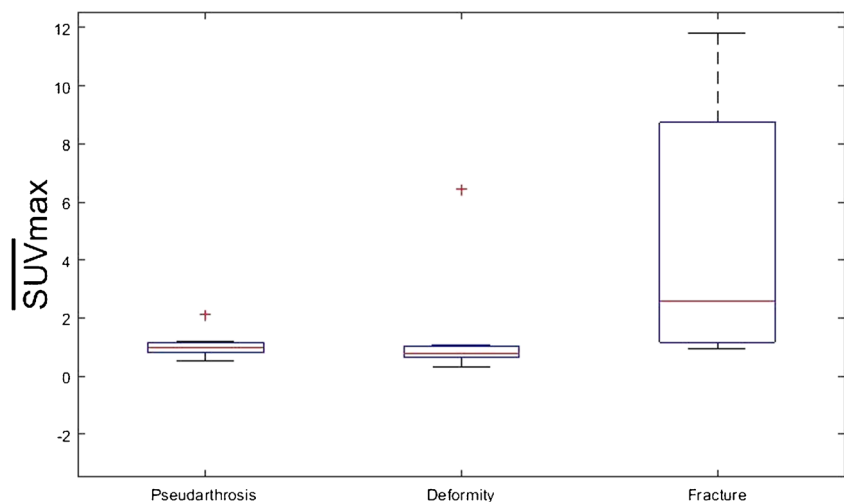


Table 2 Confusion matrix for the Taylor spatial frame (TSF) treatment outcome prediction according to [¹⁸F]-fluoride-PET described by $\bar{K}_{i,max}$ (ratio of the maximum plasma to bone fluoride net influx rate at PET scan 2 and 1)

		n = 21	
		[¹⁸ F]fluoride-PET predicted TSF treatment outcome	
		Positive	Negative
Clinical TSF treatment outcome	Positive	8	4
	Negative	2	7

course of the study [22, 23]. This limited value of SUV for quantification of [¹⁸F]-fluoride-PET has also been previously reported in treatment of osteoporosis [24] and in patients after resection of bone tumors of the limb and bone graft surgery [14].

To the best of our knowledge, we provide for first time, evidence that [¹⁸F]-fluoride-PET parametric images of $\bar{K}_{i,max}$ may be used for both discriminating orthopedic conditions ($p = 0.0046$) and monitoring the bone remodeling process. We also found a significant predictive value between the temporal changes in [¹⁸F]-fluoride influx rate $\bar{K}_{i,max}$ (at 4 months post TSF installation) and the healing progression and clinical treatment outcome. Patients with an arrested osteoblastic activity, as reflected by the [¹⁸F]-fluoride $\bar{K}_{i,max}$ in bone, also clinically-radiologically showed delayed bone repair, the longer TSF treatment period, pain and loss of mobility after TSF treatment. This important feature of [¹⁸F]-fluoride is lost when using SUV-based static PET imaging. This is not surprising because of the well-known bias in PET tracer quantification introduced by SUV, as previously mentioned.

Another critical point in this type of correlative analysis is the choice of a scoring system to objectively describe the clinical TSF treatment outcome. In this respect, radiological scoring of callus formation is subjective and, additionally, in the current setting, subject to the course of external manipulation of the TSF struts during treatment (because mechanical stress may delay the offset of callus formation.) However, the

Table 3 Confusion matrix for the Taylor spatial frame (TSF) treatment outcome prediction according to [¹⁸F]-fluoride-PET described by \bar{SUV}_{max} (ratio of the maximum Standard Uptake Value at PET scan 2 and 1)

		n = 21	
		[¹⁸ F]fluoride-PET predicted TSF treatment outcome	
		Positive	Negative
Clinical TSF treatment outcome	Positive	3	9
	Negative	6	3

other four clinical end points used in the scoring system, pain, extremity mobility, infection, and number of days during TSF treatment compared to the mean of the group, are more robust descriptors for the treatment outcome.

Except for the technical limitations previously discussed, this study comprised a small number of patients and inclusion of three orthopedic conditions on which TSF treatment was applied and calls for a larger longitudinal multicenter study.

Conclusion

To conclude, $\bar{K}_{i,max}$ obtained from dynamic [¹⁸F]-fluoride-PET imaging is a promising predictive factor to evaluate changes in bone healing in response to TSF treatment. These results suggest that the specific bone-phenotype described by the rate of bone healing could be monitored using $\bar{K}_{i,max}$ of [¹⁸F]-fluoride from dynamic PET/CT imaging, which may facilitate the management of patients treated with TSF.

Compliance with ethical standards

Conflict of interest A. Sanchez-Crespo declares that he has no conflict of interest.

F. Christiansson declares that he has no conflict of interest.

C. K. Thur declares that she has no conflict of interest.

H. Lundblad declares that he has no conflict of interest.

A. Sundin declares that he has no conflict of interest.

Ethical approval All procedures performed in this work involving human participants were in accordance with the ethical standards of the institutional and/or national research committee and with the 1964 Helsinki Declaration and its later amendments or comparable ethical standards.

Informed consent Informed consent was obtained from all individual participants included in the study.

References

- Charles JT. Correction of general deformity with the Taylor Spatial Frame fixator. General TSF literature. 2002. <http://www.jcharlestaylor.com/tsfliterature/01TSF-mainHO.pdf> Accessed 21 Dec 2015.
- Tan B, Shanmugam R, Gunalan R, Chua Y, Hossain G, Saw A. A biomechanical comparison between Taylor's Spatial Frame and Ilizarov external fixator. *Malays Orthop J*. 2014;8:35–9.
- Rozbruch SR, Segal K, Ilizarov S, Fragomen AT, Ilizarov G. Does the Taylor spatial frame accurately correct tibial deformities? *Clin Orthop Relat Res*. 2010;468:1352–61.
- Kuhlman JE, Fishman EK, Magid D, Scott Jr WW, Brooker AF, Siegelman SS. Fracture nonunion: CT assessment with multi-planar reconstruction. *Radiology*. 1988;167:483–8.
- Bockisch A, Beyer T, Antoch G, Freudenberg LS, Kühl H, Debatin JF, et al. Positron emission tomography/computed tomography–imaging protocols, artifacts and pitfalls. *Mol Imaging Biol*. 2004;6:188–99.

6. Schäfers K, Raupach R, Beyer T. Combined 18F-FDG-PET/CT imaging of the head and neck: an approach to metal artifact correction. *Nuklearmedizin*. 2006;45:219–22.
7. Hsu WK, Feeley BT, Krenek L, Stout DB, Chatziioannou AF, Lieberman JR. The use of 18F-fluoride and 18F-FDG PET scans to assess fracture healing in a rat femur model. *Eur J Nucl Med Mol Imaging*. 2007;34:1291–301.
8. Blake GM, Park-Holohan SJ, Fogelman I. Quantitative studies of bone in postmenopausal women using ¹⁸F-fluoride and ^{99m}Tc-methylene diphosphonate. *J Nucl Med*. 2002;43:338–45.
9. Installé J, Nzeusseu A, Bol A, Depresseux A, Devogelaer JP, Lonneux M. 18F-fluoride PET for monitoring therapeutic response in Paget's disease of bone. *J Nucl Med*. 2005;46(10):1650–8.
10. Messa C, Goodman WG, Hoh CK, et al. Bone metabolic activity measured with positron emission tomography and [¹⁸F]-fluoride ion in renal osteodystrophy: correlation with bone histomorphometry. *J Clin Endocrinol Metab*. 1993;77:949–55.
11. Piert M, Zittel TT, Becker GA, et al. Assessment of porcine bone metabolism by dynamic [¹⁸F]-fluoride ion PET: correlation with bone histomorphometry. *J Nucl Med*. 2001;42:1091–100.
12. Hawkins RA, Choi Y, Huang SC, Hoh CK, Dahlbom M, Schiepers C, et al. Evaluation of the skeletal kinetics of fluorine-18-fluoride ion with PET. *J Nucl Med*. 1992;33:633–42.
13. Segall G, Delbeke D, Stabin MG, Even-Sapir E, Fair J, Sajdak R, et al. SNM practice guideline for sodium 18F-fluoride PET/CT bone scans 1.0. *J Nucl Med*. 2010;51:1813–20.
14. Brenner W, Vernon C, Muzi M, Mankoff DA, Link JM, Conrad EU, et al. Comparison of different quantitative approaches to 18F-fluoride PET scans. *J Nucl Med*. 2004;45:1493–500.
15. Doot RK, Muzi M, Peterson LM, Schubert EK, Gralow JR, Specht JM, et al. Kinetic analysis of ¹⁸F-fluoride PET images of breast cancer bone metastases. *J Nucl Med*. 2010;51:521–7.
16. Patlak CS, Blasberg RG, Fenstermacher JD. Graphical evaluation of blood-to-brain transfer constants from multiple-time uptake data. *J Cereb Blood Flow Metab*. 1983;3:1–7.
17. Hatherly R, Brodin F, Oldner Å, Sundin A, Lundblad H, Maguire Jr GQ, et al. Technical requirements for Na¹⁸F PET bone imaging of patients being treated using a Taylor spatial frame. *J Nucl Med Technol*. 2014;42:33–6.
18. Wen L, Eberl S, Dagan Feng D, Stalley P, Huang G, Fulham MJ. Parametric images in assessing bone grafts using dynamic ¹⁸F-Fluoride PET. *Int J Mol Imaging*. 2011;2011, 189830.
19. Blomqvist G. On the construction of functional maps in positron emission tomography. *J Cereb Blood Flow Metab*. 1984;4:629–32.
20. Sanchez-Crespo A. Comparison of Gallium-68 and Fluorine-18 imaging characteristics in positron emission tomography. *Appl Radiat Isot*. 2013;76:55–62.
21. Boellaard R, Delgado-Bolton R, Oyen WJ. FDG PET/CT: EANM procedure guidelines for tumour imaging: version 2.0. *Eur J Nucl Med Mol Imaging*. 2015;42(2):328–54.
22. Temmerman OP, Raijmakers PG, Kloet R, Teule GJ, Heyligers IC, Lammertsma AA. In vivo measurements of blood flow and bone metabolism in osteoarthritis. *Rheumatol Int*. 2013;33(4):959–63.
23. Blake GM, Frost ML, Fogelman I. Quantitative radionuclide studies of bone. *J Nucl Med*. 2009;50(11):1747–50.
24. Blake GM, Siddique M, Frost ML, Moore AE, Fogelman I. Radionuclide studies of bone metabolism: do bone uptake and bone plasma clearance provide equivalent measurements of bone turnover? *Bone*. 2011;49(3):537–42.